CLINICAL IMAGE

Tumor-induced hypophosphatemic osteomalacia as a rare cause of bone pain

Sebastian Spaleniak[1], Grzegorz Kade[1], Rafał Kidziński[2], Andrzej Mazurek[3], Arkadiusz Lubas[1], Stanisław Niemczyk[1]

1 Department of Internal Medicine, Nephrology and Dialysis, Military Institute of Medicine, Warsaw, Poland
2 Department of Radiology, Military Institute of Medicine, Warsaw, Poland
3 Department of Nuclear Medicine, Military Institute of Medicine, Warsaw, Poland

A 49-year-old female patient in a good general condition was admitted due to pain in the attachments of the lower ribs to the sternum, distal femurs, tibias, and fibulas, as well as lower limb muscles, persisting for 3 years. Medical history revealed hyperthyroidism treated with radioiodine therapy a few years earlier. Because of subsequent hypothyroidism, the patient additionally used levothyroxine. Her serum phosphate levels were reduced for the past 2 years (1.17–1.7 mg/dl; reference range, 2.7–4.5 mg/dl). The family history was negative for hypophosphatemia. Based on an interview and clinical data, we had no reason to suspect increased phosphate displacement from the extracellular to intracellular space due to hypophosphatemia.

Because of a suspected phosphorus loss in urine, daily urine collection was performed; a tubular reabsorption of phosphate was 62% (reference range >86%). The ratio of the tubular maximum reabsorption of phosphate was 0.87 mg/dl (reference range, 3.0–5.0 mg/dl).[1] The results confirmed renal phosphate wasting. The serum concentrations of sodium, potassium, calcium, magnesium, parathyroid hormone, alkaline phosphatase, and creatinine were normal. The levels of venous blood gases, $25(OH)D_3$, $1,25(OH)_2D_3$, as well as the results of complete blood count and urinalysis, were normal.

Considering other causes of hypophosphatemia, we tested the patient for oncogenic hypophosphatemia, using abdominal ultrasound, gastrointestinal endoscopy, mammography, and classic chest X-ray.[2] Skeletal scintigraphy with ^{99m}Tc with methylene diphosphonate using the planar method, together with single-photon emission computed tomography and computed tomography, was also performed. The examinations revealed multiple foci of excessive tracer accumulation (FIGURE 1A–1C). These sites were marked using conventional radiographs (FIGURE 1D and 1E), which showed pseudofractures, the so called Looser–Milkman zone (FIGURE 1D).[3]

To enhance the diagnostic workup, exon 3 and the adjacent intron of the gene sequences of fibroblast growth factor 23 (FGF-23) had been analyzed using DNA sequencing. There were no signs of the pathogenic variants c.527G> A p. Arg176Gln; c.526C>T p.Arg176Trp: c.536G>A p.Arg179Gln, and c.535C>T p.Arg179Trp that would explain the clinical symptoms of hypophosphatemic rickets.[5] Serum FGF-23 concentrations were 356 kRU/l (reference range, 26–110 kRU/l).

The patient was put on diet with relevant phosphate supplementation (a mixture of Na_2HPO_4 and NaH_2PO_4, and additional calcium). A gradual clinical improvement and an increase in the phosphate concentration were observed. Skeletal scintigraphy at approximately 2-year follow-up showed significant bone lesions (FIGURE 1B). However, due to persistent hypophosphatemia and elevated FGF-23 concentrations despite the resolution of symptoms, we decided to perform another scintigraphy using somatostatin analogs. Somatostatin receptors type 2 and 5 were clearly visible in the occipital region (FIGURE 1F and 1G), suggesting mesenchymal cancer producing the phosphaturic factor.[4,5] We performed ^{18}F-fluorodeoxyglucose positron emission tomography / computed tomography, which confirmed the tumor site and its malignant type (FIGURE 1H–1J). Magnetic resonance imaging showed features of pathological tumor vascularization (Supplementary material, *Figure S1*).

Due to the biological behavior of the tumor-induced hypophosphatemic osteomalacia and its rare incidence, a comprehensive evaluation of medical, laboratory, and radiographic findings is crucial for a definitive diagnosis.

Correspondence to:
Sebastian Spaleniak, MD, PhD, Klinika Chorób Wewnętrznych, Nefrologii i Dializoterapii, Wojskowy Instytut Medyczny w Warszawie, ul. Szaserów 128, 04-141 Warszawa, Poland, phone: +48 261 817 072, email: sebastian19860@op.pl
Received: January 7, 2018.
Revision accepted: March 9, 2018.
Published online: March 29, 2018.
Conflict of interests: none declared.
Pol Arch Intern Med. 2018; 128 (3): 189-191
doi:10.20452/pamw.4234

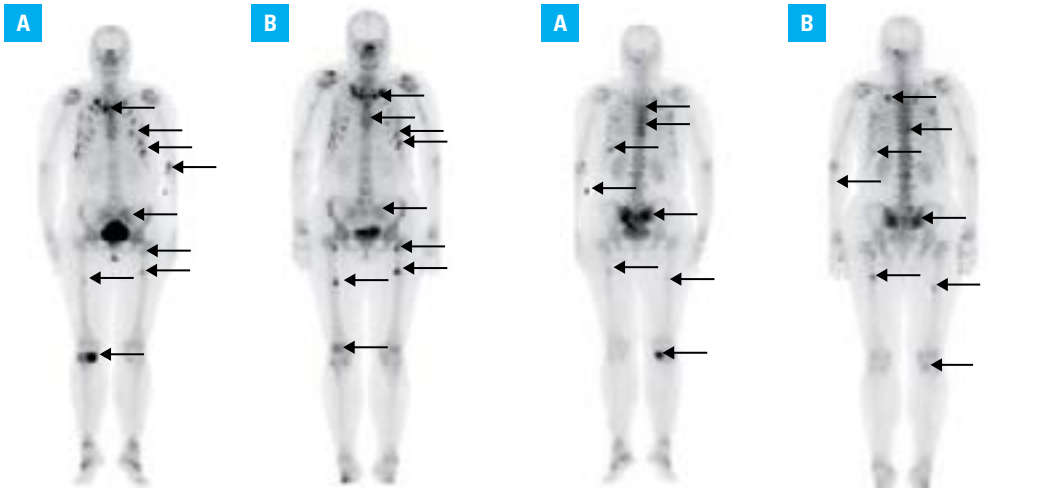

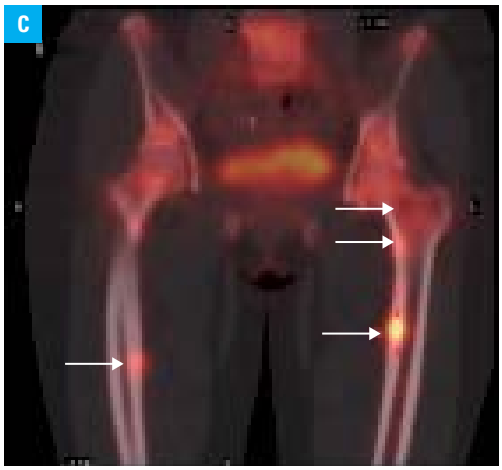

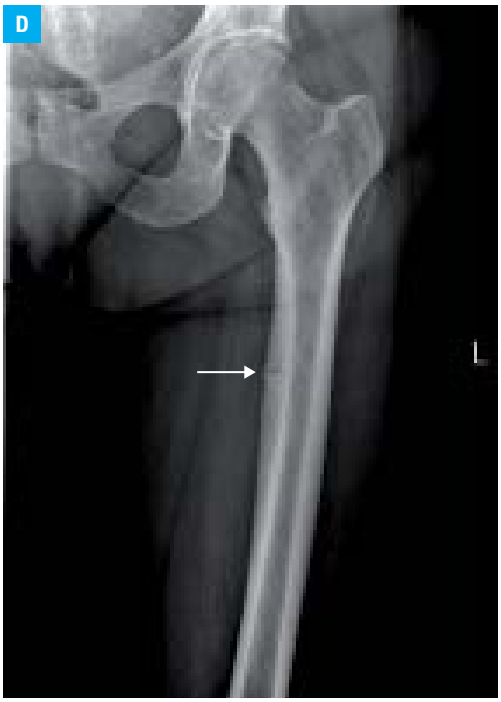

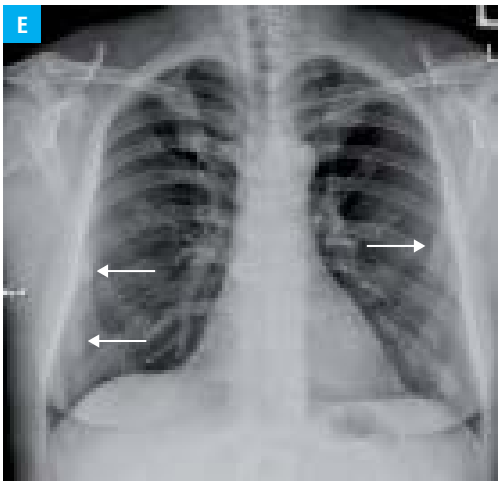

FIGURE 1 **A** – skeletal scintigraphy (2013) showing foci of increased osteotropic marker accumulation in the ribs on the front and back sides of the chest, at the lesser trochanter and in the shafts of both femurs, uneven marker collection within vertebrae Th3–Th9 in the spine, diffuse accumulation in sacroiliac joints, large intensive foci in the front and medial condyles of the right tibia (arrows); **B** – skeletal scintigraphy (2015) showing a lower uptake of osteotropic marker in the ribs, slightly more intense uptake in the focus at the lesser trochanter and the foci in the shafts of both femurs, uneven and lower uptake in the spine (invisible collection in Th3–Th9), slightly increased accumulation in the sacroiliac joints, lower uptake in the medial condyle of the right tibia; a new focus on the smaller right trochanter of the femur and the lateral femoral condyle (arrows); **C** – single-photon emission computed tomography and computed tomography (2013), front projection: increased uptake in the osteotropic marker inside the thickened cortex of femur shafts (arrows); **D** – left femur X-ray visible focal Looser–Milkman zone in the thickened cortex of the vertebral body (arrow); **E** – chest X-ray: history of broken ribs VI and VII on the right side and rib V on the left side (arrows); visible bone junctions with the local reconstruction of the bone at the site of fracture (arrows)

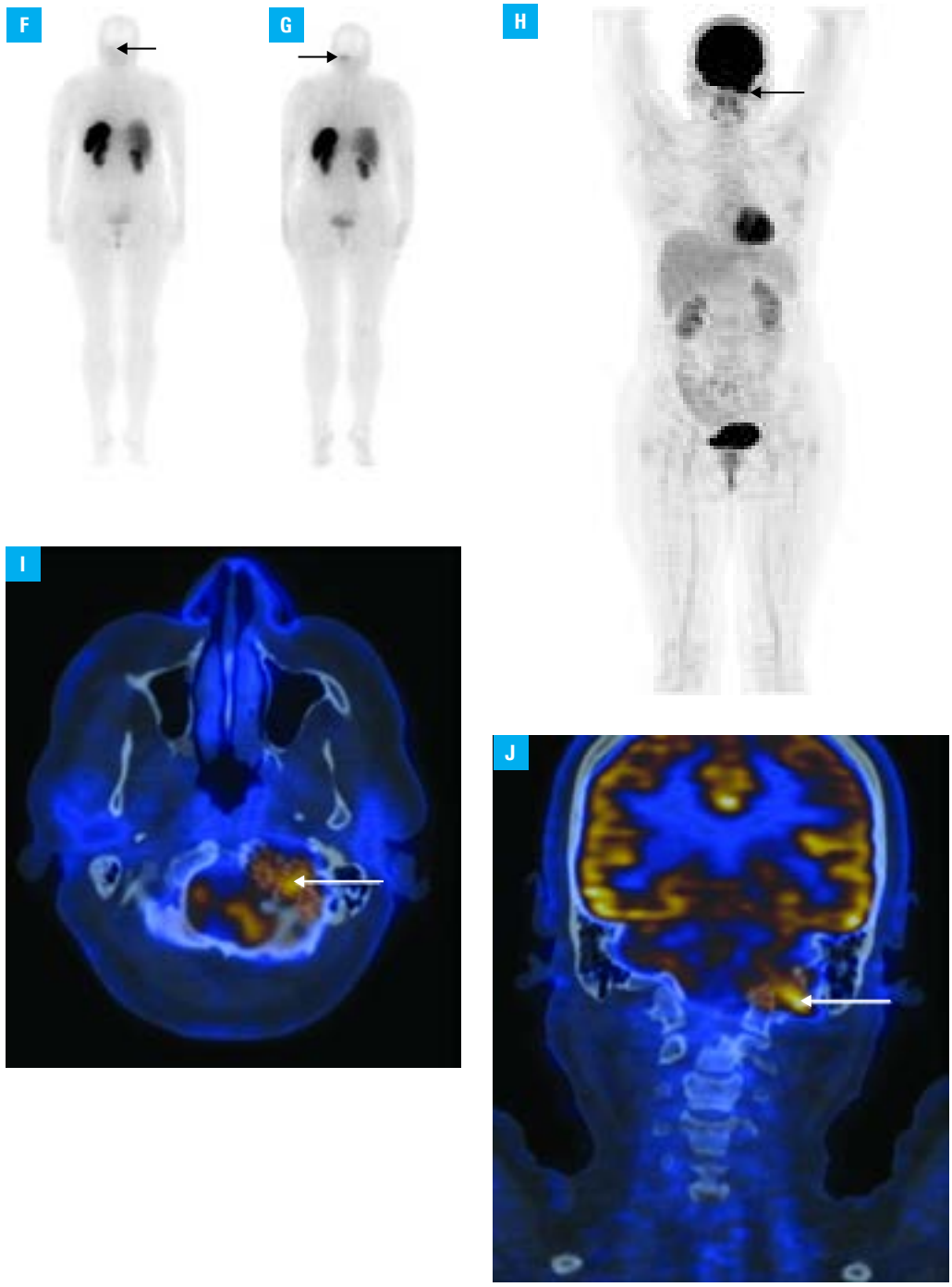

FIGURE 1 **F** and **G** – somatostatin receptor scintigraphy: **G** (2017) in comparison to **F** (2015) showed increased uptake in the left occipital region (arrows); **H** – maximum intensity projection positron emission tomography scan showing focal ^{18}F-fluorodeoxyglucose (FDG) uptake in the left occipital region (arrow); **I** – axial positron emission tomography / computed tomography (PET/CT) scan showing FDG uptake and osteolytic lesion in the left occipital region (arrow); **J** – coronal PET/CT scan showing FDG uptake and osteolytic lesion in the left occipital region (arrow)

SUPPLEMENTARY MATERIAL Supplementary material is available with the online version of the article at www.pamw.pl.

REFERENCES

1 Payne RB. Renal tubular reabsorption of phosphate, (TmP/GFR): indications and interpretation. Ann Clin Biochem. 1998; 35: 201-206.

2 Krela-Kaźmierczak I, Szymczak A, Tomczak M, et al. Calcium and phosphate metabolism in patients with inflammatory bowel diseases. Pol Arch Med Wewn. 2015; 125: 588-590.

3 Siegel HJ, Rock MG, Inwards C, Sim FH. Phosphaturic mesenchymal tumor. Orthopedics. 2002; 25: 1279-1281.

4 Reubi JC, Waser B, Laissue JA, et al. Somatostatin and vasoactive intestinal peptide receptors in human mesenchymal tumors: in vitro identification. Cancer Res. 1996; 56: 1922-1931.

5 Strewler GJ. FGF23, hypophosphatemia, and rickets: has phosphatonin been found? Proc Natl Acad Sci USA. 2001; 98: 5945-5946.